IOP PUBLISHING JOURNAL OF PHYSICS A: MATHEMATICAL AND THEORETICAL

J. Phys. A: Math. Theor. **42** (2009) 214020 (12pp) doi:10.1088/1751-8113/42/21/214020

# Nonequilibrium properties of strongly correlated artificial atoms—a Green's functions approach

**K Balzer and M Bonitz**

Institut für Theoretische Physik und Astrophysik, Christian-Albrechts-Universität Kiel, Leibnizstrasse 15, 24098 Kiel, Germany

E-mail: balzer@theo-physik.uni-kiel.de

Received 15 October 2008, in final form 11 December 2008
Published 8 May 2009
Online at stacks.iop.org/JPhysA/42/214020

**Abstract**

A nonequilibrium Green's functions (NEGF) approach for spatially inhomogeneous, strongly correlated artificial atoms is presented and applied to compute the time-dependent properties starting from a (correlated) initial few-electron state at finite temperatures. In the regime of moderate-to-strong coupling, we consider the Kohn mode of a three-electron system in a parabolic confinement excited by a short-pulsed classical laser field treated in the dipole approximation. In particular, we numerically confirm that this mode is preserved within a conserving (e.g., Hartree–Fock or second Born) theory.

PACS numbers: 05.30.−d, 73.21.−b

## 1. Introduction

'Artificial atoms' (AA) are inhomogeneous quantum few-particle Coulomb systems confined in a trapping potential and show bound discrete electronic states, as they are occurring in real atoms [1]. Most artificial atoms are realized in an (isotropic) parabolic confinement, and quantum dots are a synonym convention for these systems, e.g., [2, 3]. But AAs are also formed by ions in Penning and Paul traps [4, 5], charge carriers in semiconductor heterostructures [6–8] (quantum wells) or electrons in metal clusters [9, 10]. AAs in one- (1D) and two-dimensional (2D) entrapment show interesting properties far from ideal Fermi-gas behavior including ring and shell structures—see the 2D ground-state configurations for $N = 2, 3, \ldots, 7$ electrons displayed in figure 1. This is due to the externally controllable electron–electron interactions which can lead to the formation of strongly coupled systems including correlation phenomena.

Previous theoretical investigations of AAs mainly concern ground-state calculations and approaches to thermodynamic equilibrium; see [3, 6] and references therein. The aim of this paper is to present a time-dependent theory including moderate and strong correlations. Following a quantum statistical approach, we thereby want to consider the system's response

  

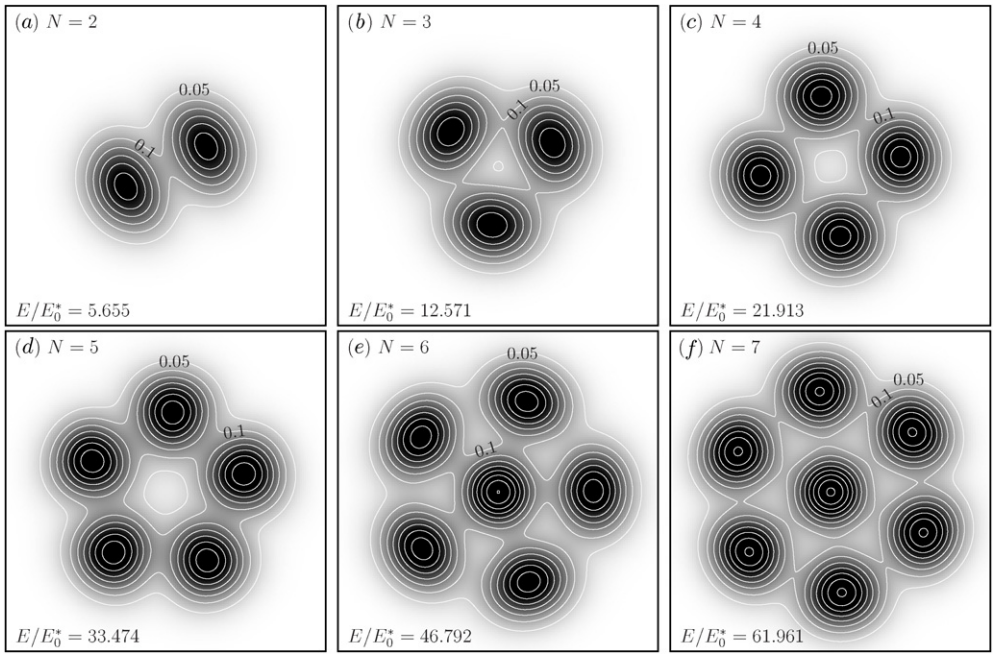


**Figure 1.** Examples for the one-electron ground-state (GS) density $n_N^{\mathrm{GS}}(\mathbf{r})$ of $N = 2, 3, \ldots, 7$ electrons in an isotropic 2D trap for $\beta = 100$ and $\lambda = 5.0$. Figures $(a)$–$(f)$ display the result of (symmetry broken) Hartree–Fock calculations. The side length of the density plots measures $8x_0^*$ with $x_0^* = \sqrt{\hbar/(m_e^*\omega_0)}$ and $E_0^* = \hbar\omega_0$.

to a (strong) short-pulsed laser field while being embedded into an environment of finite temperature. To this end, in sections 3 and 4, we describe the NEGF method applied to compute the (correlated) initial state which is then propagated in time according to the Keldysh/Kadanoff–Baym equations. In section 5, we present results for a three-electron AA in a 1D and 2D trap geometry.

## 2. Model

The $d$-dimensional $N$-electron Hamiltonian of an artificial atom in a time-dependent laser field $\mathbf{E}(t)$ described in the dipole approximation reads

$$\hat{H}(t) = \sum_{i=1}^{N}\left(-\frac{\hbar^2}{2m_e^*}\nabla_i^2 + \frac{m_e^*}{2}\omega_0^2\mathbf{r}_i^2 + e\mathbf{E}(t)\mathbf{r}_i\right) + \sum_{i<j}^{N}\frac{e^2}{4\pi\varepsilon r_{ij}}, \tag{1}$$

where the effective electron mass is given by $m_e^*$, the frequency $\omega_0$ adjusts the confinement strength (and hence the density in the AA), $e$ is the elementary charge, and $\varepsilon = \varepsilon_0\varepsilon_b$ denotes the background dielectric constant where $\varepsilon_b \approx 10$ is typical for semiconductor materials. Further, the $d$-dimensional electron coordinates $\mathbf{r}_i$ originate from the trap center and $r_{ij} = |\mathbf{r}_i - \mathbf{r}_j|$.

Hamiltonian (1) can be rewritten in a dimensionless form, using the transformations $\{E \to E/E_0^*, \mathbf{r} \to \mathbf{r}/x_0^*\}$, where $E_0^* = \hbar\omega_0$ is the confinement energy and the (oscillator) length $x_0^* = \sqrt{\hbar/(m_e^*\omega_0)}$ denotes the characteristic spatial one-electron extension in the AA.

Consequently, the system is characterized by a single coupling (or Wigner) parameter $\lambda$, which relates the characteristic Coulomb energy $E_C = e^2/(4\pi\varepsilon x_0^*)$ to $E_0^*$ according to

$$\lambda = \frac{E_C}{E_0^*} = \frac{e^2}{4\pi\varepsilon x_0^* \hbar\omega_0} = \frac{x_0^*}{a_B}, \tag{2}$$

with $a_B$ being the effective electron Bohr radius. Hamiltonian (1) then transforms into the dimensionless form

$$\hat{H}_\lambda(t) = \frac{1}{2}\sum_{i=1}^{N}\left(-\nabla_i^2 + \mathbf{r}_i^2 + \gamma(t)\mathbf{r}_i\right) + \lambda\sum_{i<j}^{N}\frac{1}{r_{ij}}, \tag{3}$$

with $\gamma(t) = eE(t)/\sqrt{\hbar m_e^* \omega_0}$. The coupling parameter $\lambda$ adjusts the influence of electron–electron interactions and (quantum) correlations. In the case of $\lambda \ll 1$, the artificial atom behaves similar to an ideal Fermi gas. For $\lambda \sim 1$, the equilibrium state of the AA is Fermi liquid like, whereas in the limit $\lambda \to \infty$, it is $x_0^* \gg a_B$, and quantum effects vanish in favor of classical interaction dominated charge carriers [19]. For moderate coupling ($\lambda \gtrsim 1$) the AAs typically show spatially well-localized carrier density including Wigner molecule (Wigner crystal-like) behavior [6]; see figure 1. Moreover, if the AA is not in its ground state (GS), one has to take into account thermodynamic fluctuations due to a surrounding heat bath of dimensionless temperature $\beta^{-1} = k_B T/E_0^*$. Below, all presented results are related to the system of units $\{x_0^*, E_0^*\}$ and in the definition of the NEGFs we take $\hbar = 1$.

## 3. Preparation of equilibrium states

Introducing electron annihilation (creation) operators $\psi^{(\dagger)}(\mathbf{r}_1 t_1)$ acting in the Heisenberg picture at a spacetime point $1 = (\mathbf{r}_1, t_1)$, the second-quantized form of (3) reads

$$H_\lambda(t_1) = \int \mathrm{d}^{\mathrm{d}} r\, \hat{\psi}^\dagger(1) h^0(1) \hat{\psi}(1) + \iint \mathrm{d}^{\mathrm{d}} r\, \mathrm{d}^{\mathrm{d}} \bar{r}\, \hat{\psi}^\dagger(1)\hat{\psi}^\dagger(\bar{1}) w(\mathbf{r}_1 - \mathbf{r}_{\bar{1}})\hat{\psi}(\bar{1})\hat{\psi}(1), \tag{4}$$

with the one-electron energy $h^0(1) = \left(-\nabla_{r_1}^2 + \mathbf{r}_1^2\right)/2 + \gamma(t_1)\mathbf{r}_1$ and the interaction $w(\mathbf{r}_1 - \mathbf{r}_{\bar{1}}) = \lambda|\mathbf{r}_1 - \mathbf{r}_{\bar{1}}|^{-1}$ including a second spacetime point $\bar{1} = (\mathbf{r}_{\bar{1}}, t_{\bar{1}})$. In the following, we study Hamiltonian (4) at finite temperatures $\beta^{-1}$ by means of the one-particle nonequilibrium Green function $G(1, \bar{1})$, which is defined on the Schwinger/Keldysh contour $\mathcal{C}$ (see, e.g., [11, 12]) as

$$G(1, \bar{1}) = -\mathrm{i}\langle T_{\mathcal{C}} \hat{\psi}(1)\hat{\psi}^\dagger(\bar{1})\rangle, \tag{5}$$

where $T_{\mathcal{C}}$ denotes time ordering on $\mathcal{C}$. $G(1, \bar{1})$ obeys the two-time Keldysh/Kadanoff–Baym equation (KBE) [13]:

$$[\mathrm{i}\partial_{t_1} - h(1)]G(1, \bar{1}) = \delta_{\mathcal{C}}(1 - \bar{1}) - \mathrm{i}\int_{\mathcal{C}} \mathrm{d}2\, W(1 - 2)G_{12}(1, 2; \bar{1}, 2^+), \tag{6}$$

and its adjoint, where $W(1 - \bar{1}) = \delta_{\mathcal{C}}(t_1 - t_{\bar{1}})w(\mathbf{r}_1 - \mathbf{r}_{\bar{1}})$ acts instantaneously with the contour delta function $\delta_{\mathcal{C}}$, and $2^+$ indicates the time limit $t_2 \to t_2 + 0$. Here, the two-particle Green function,

$$G_{12}(1, 2; \bar{1}, \bar{2}) = (-\mathrm{i})^2\langle T_{\mathcal{C}} \hat{\psi}(1)\hat{\psi}(2)\hat{\psi}^\dagger(\bar{2})\hat{\psi}^\dagger(\bar{1})\rangle, \tag{7}$$

appears as a generalization of the two-particle density matrix. In terms of $G_{12}$, we can formulate all relevant many-body approximations. For instance, substituting $G_{12}(1, 2; \bar{1}, \bar{2}) \to G(1, \bar{1})G(2, \bar{2}) - G(1, \bar{2})G(2, \bar{1})$ yields the Hartree–Fock (HF) approximation. Second- and higher-order approximations for $G_{12}$ generally include

integrations over a four-point vertex function $\Gamma$ [15], and can be reformulated in terms of a self-energy $\Sigma$ accessible by diagram expansions known from ground-state many-body theory.

When in equation (4), we consider $\gamma(t_1) \equiv 0$ for $-\infty < t_1 \leqslant t_0$, the AA stays in thermodynamic equilibrium until at a time $t_1 > t_0$ $\gamma(t_1)$ becomes nonzero. Without loss of generality we thereby can take $t_0 = 0$. Specifying the time-independent single-electron part of equation (4) as $h^0(\mathbf{r}_1) = h(1)|_{\gamma(t_1)=0}$, the KBE then reduces, for $t_{1,\bar{1}} \leqslant 0$, to the Dyson equation

$$[-\partial_\tau - h^0(\mathbf{r}_1)]G^M(\mathbf{r}_1, \mathbf{r}_{\bar{1}}; \tau) = \delta(\tau) + \int \mathrm{d}^2\bar{r} \int_0^\beta \mathrm{d}\bar{\tau}\, \Sigma_\lambda^M(\mathbf{r}_1, \bar{\mathbf{r}}; \tau - \bar{\tau}) G^M(\bar{\mathbf{r}}, \mathbf{r}_{\bar{1}}; \bar{\tau}). \tag{8}$$

Here, the Matsubara Green's function being defined as $G^M(1, \bar{1}) = G^M(\mathbf{r}_1, \mathbf{r}_{\bar{1}}; \tau) = G(\mathbf{r}_1 0 - \mathrm{i}\tau_1, \mathbf{r}_{\bar{1}} 0 - \mathrm{i}\tau_{\bar{1}})$, with $\tau = \tau_1 - \tau_{\bar{1}} \in [-\beta, \beta]$, characterizes the equilibrium (initial) state of the AA. Further, on the right-hand side, we have introduced the self-energy $\Sigma_\lambda^M(1, \bar{1}) = \Sigma_\lambda^M(\mathbf{r}_1, \mathbf{r}_{\bar{1}}; \tau)$ according to $-\mathrm{i}W(1-2)G_{12}(1, 2; \bar{1}, 2^+)|_{t_{1,\bar{1}} \leqslant 0} = \Sigma[G](1, 2)G(2, \bar{1})$. A conserving many-body approximation [13], i.e. an approximation for $\Sigma$ that preserves density (continuity equation), total energy and momentum, can be systematically derived from a functional $\Phi$ such that $\Sigma(1, \bar{1}) = \delta\Phi[G]/\delta G(\bar{1}, 1)$. Important examples, being second and higher order in the interaction $W(1, \bar{1})$, are self-energies of second Born [3], $GW$ or $T$-matrix type [13, 14]. Below, we consider the $\Phi$-derivable HF and second Born approximation, while applying a fully self-consistent $GW$ scheme [16] that accounts for a dynamically screened Coulomb interaction, summing up an infinite series of ring diagrams, is the subject of future work.

At a given temperature $\beta^{-1}$, most of the equilibrium properties of the AA system (1), e.g. total energy, one-particle density and energy spectrum, are contained in $G^M$; see the formulae in section 4.2 and take the limit $t_1 \to 0$. For the numerical techniques applicable in solving equation (8) in a matrix form, see, e.g., [3, 17, 18]. In the HF approximation, the self-consistent solution can be written as

$$\begin{aligned} G^M(\mathbf{r}_1, \mathbf{r}_{\bar{1}}; \tau) &= \sum_{m=0}^{n_b-1} \phi_m^*(\mathbf{r}_1)\phi_m(\mathbf{r}_{\bar{1}}) g_{mm}^M(\tau), \\ g_{mm}^M(\tau) &= f_\beta(\epsilon_m - \mu)\, \mathrm{e}^{-\tau(\epsilon_m - \mu)} = \mathrm{e}^{-\tau(\epsilon_m-\mu)}/(\mathrm{e}^{\beta(\epsilon_m-\mu)} + 1), \end{aligned} \tag{9}$$

with interaction-renormalized (effective single-electron) HF orbitals $\phi_m(\mathbf{r})$ [19], quantum numbers $m = 0, \ldots, n_b - 1$, discrete energies $\epsilon_m$ and a chemical potential $\mu$. Beyond the HF level, $G^M$ will be no longer diagonal in the functions $\phi_m$, and the respective occupation probabilities will deviate from a Fermi–Dirac distribution, $f_\beta(\epsilon_m - \mu)$, due to additional electron scattering processes. In particular, the inclusion of electron–electron correlations leads to orbital-dependent energy shifts and broadening in the HF spectrum $a(\omega) = \sum_m \delta(\omega - \epsilon_m)$; see [3].

## 4. Time propagation of initial states

When for $t_1 > 0$ the laser field is switched on and $\gamma(t_1) \neq 0$, the quantum state of the AA evolves in real time according to the KBE, equation (6) and its adjoint. Thereby, being computed from the Dyson equation (8) in a self-consistent manner, the Matsubara Green's function serves as an initial (Kubo–Martin–Schwinger) condition for the time propagation. In particular, for $t_0 = 0$, one has

$$G(\mathbf{r}_1 0 - \mathrm{i}\tau_1, \mathbf{r}_{\bar{1}} 0 - \mathrm{i}\tau_{\bar{1}}) = \mathrm{i}[G^M(\mathbf{r}_1, \mathbf{r}_{\bar{1}}; \tau_1) - G^M(\mathbf{r}_1, \mathbf{r}_{\bar{1}}; -\tau_{\bar{1}})]. \tag{10}$$

Beyond the mean-field level, all relevant initial correlations are taken into account via $G^M$ and, consequently, evolve in time, leading to a correlated $N$-particle dynamics.

### *4.1. Solving the Keldysh/Kadanoff–Baym equations*

The expansion of the NEGF in terms of a HF basis, see equation (9), also advises us to solve the real-time KBE in a matrix form [17, 20]. This means that we generally consider

$$G(1,\bar{1}) = \sum_{m,n=0}^{n_b-1} \phi_m^*(\mathbf{r}_1)\phi_n(\mathbf{r}_{\bar{1}})g_{mn}(t_1,t_{\bar{1}}), \tag{11}$$

with time arguments $t_1, t_{\bar{1}}$ on the contour $\mathcal{C}$, the coefficient matrix $g_{mn}(t_1,t_{\bar{1}}) = \theta(t_1,t_{\bar{1}})g^{>}_{mn}(t_1,t_{\bar{1}}) - \theta(t_{\bar{1}},t_1)g^{<}_{mn}(t_1,t_{\bar{1}})$ of dimension $n_b \times n_b$, and steady-state HF orbitals $\phi_m(\mathbf{r})$ which generate a complete orthonormal set. Hence, $g_{mn}(t_1,t_{\bar{1}}) = -\mathrm{i}\langle T_{\mathcal{C}} c_m(t_1)c_n^\dagger(t_{\bar{1}})\rangle$ are just the NEGFs with respect to the operators $\hat{c}_m^\dagger$ ($\hat{c}_m$) that create (annihilate) an electron in the state $m$. Consequently, the diagonal elements $[m = n]$ are directly related to the occupation numbers (probabilities) of the HF orbitals, cf equation (17), whereas the off-diagonal elements $[m \neq n]$ are connected with 'interband' excitations, i.e. the transition probabilities between the energy levels.

Inserting expression (11), equation (6) and its adjoint then transform into integro-differential equations for the matrix elements $g_{mn}(t_1,t_{\bar{1}}) = (\mathbf{g})_{mn}(t_1,t_{\bar{1}})$:

$$[\mathrm{i}\partial_{t_1} - \mathbf{h}(t_1)]\mathbf{g}(t_1,t_{\bar{1}}) = \delta_{\mathcal{C}}(t_1 - t_{\bar{1}}) + \int_{\mathcal{C}} \mathrm{d}\bar{t}\, \boldsymbol{\Sigma}(t_1,\bar{t})\mathbf{g}(\bar{t},t_{\bar{1}}), \tag{12}$$

$$\mathbf{g}(t_1,t_{\bar{1}})[-\mathrm{i}\partial_{t_{\bar{1}}} - \mathbf{h}(t_{\bar{1}})] = \delta_{\mathcal{C}}(t_1 - t_{\bar{1}}) + \int_{\mathcal{C}} \mathrm{d}\bar{t}\, \mathbf{g}(t_1,\bar{t})\boldsymbol{\Sigma}(\bar{t},t_{\bar{1}}), \tag{13}$$

where the single-carrier energy is given by $h_{mn}(t_1) = \int \mathrm{d}^{\mathrm{d}} r_1\, \phi_m^*(\mathbf{r}_1)h(1)\phi_n(\mathbf{r}_1)$, and in the adjoint equation (13) the operators are acting to the left. The explicit form of the self-energy matrix $\Sigma_{mn}(t_1,t_{\bar{1}})$ at the HF level is

$$\Sigma^{\mathrm{HF}}_{mn}(t_1,t_{\bar{1}}) = -\mathrm{i}\lambda\delta_{\mathcal{C}}(t_1 - t_{\bar{1}}) \sum_{k,l=0}^{n_b-1} [w_{mn,kl} - w_{ml,kn}]g^{<}_{kl}(t_1,t_{\bar{1}}), \tag{14}$$

with the two-electron integrals $w_{mn,kl}$ defined as

$$w_{mn,kl} = \iint \mathrm{d}^{\mathrm{d}} r\, \mathrm{d}^{\mathrm{d}}\bar{r}\, \phi_m^*(\mathbf{r})\phi_k^*(\bar{\mathbf{r}})w(\mathbf{r}-\bar{\mathbf{r}})\phi_n(\mathbf{r})\phi_l(\bar{\mathbf{r}}). \tag{15}$$

The detailed structure of $\boldsymbol{\Sigma}(t_1,t_{\bar{1}}) = \boldsymbol{\Sigma}^{\mathrm{HF}}(t_1,t_{\bar{1}}) + \boldsymbol{\Sigma}^{\mathrm{corr}}(t_1,t_{\bar{1}})$ in the second (order) Born approximation is given, e.g., in [3, 20, 21].

For the real-time arguments in $\mathbf{g}(t_1,t_{\bar{1}})$, it is useful to introduce relative and center-of-mass (c.m.) variables, $t_{\mathrm{c.m.}} = (t_1 + t_{\bar{1}})/2$ and $t_{\mathrm{rel.}} = t_1 - t_{\bar{1}}$. The Green's functions with respect to the c.m. time then account for the statistical (thermodynamic) properties of the artificial atom, see definitions (16)–(19), while quantities with respect to $t_{\mathrm{rel.}}$ carry the dynamical (spectral) information, cf $a(\omega)$ as defined at the end of section 4.2. Moreover, we note that equations (12) and (13) can, in the HF approximation, be further simplified to a single-time equation involving only $t_{\mathrm{c.m.}}$. More technical and numerical details for the time propagation of the Green's function matrix are to be found in [17, 20].

### *4.2. Dynamical quantities*

The spatial one-particle density in the AA and the HF orbital-resolved occupation probability of the state $m$ are

$$\langle \hat{n} \rangle (\mathbf{r}_1, t_1) = -\mathrm{i} G(1, 1^+) = -\mathrm{i} \sum_{m,n=0}^{n_b-1} \phi_m^*(\mathbf{r}_1)\phi_n(\mathbf{r}_1) g_{mn}^<(t_1, t_1), \tag{16}$$

$$\langle \hat{n}_m \rangle (t_1) = g_{mm}^<(t_1, t_1). \tag{17}$$

In a conserving approximation, the electron number $N(t_1) = \sum_m \langle \hat{n}_m \rangle (t_1)$ in the AA is preserved in agreement with the continuity equation, i.e. $\partial_{t_1} \langle \hat{n} \rangle (1) + \mathrm{div} \langle \mathbf{j} \rangle (1) = 0$ with the current density $\langle \mathbf{j} \rangle (1) = -\frac{1}{2} \left\{ \left[ \nabla_{\mathbf{r}_1} - \nabla_{\mathbf{r}_{\bar{1}}} \right] G^<(\mathbf{r}_1 t_1, \mathbf{r}_{\bar{1}} t_1) \right\}_{\mathbf{r}_1 = \mathbf{r}_{\bar{1}}}$.

The relevant energies involved are the kinetic and the potential energy:

$$\langle \hat{E}_{\mathrm{kin+pot}} \rangle (t_1) = -\mathrm{i} \sum_{m,n=0}^{n_b-1} [t_{mn} + v_{mn}(t_1)] g_{nm}^<(t_1, t_1), \tag{18}$$

with the corresponding definitions $t_{mn} = \int \mathrm{d}^\mathrm{d} r_1 \, \phi_m^*(\mathbf{r}_1) \left[ -\nabla_{\mathbf{r}_1}^2 / 2 \right] \phi_n(\mathbf{r}_1)$ and $v_{mn}(t_1) = \int \mathrm{d}^\mathrm{d} r_1 \, \phi_m^*(\mathbf{r}_1) \left[ \mathbf{r}_1^2 / 2 + \gamma(t_1) \mathbf{r}_1 \right] \phi_n(\mathbf{r}_1)$, the HF energy

$$\langle \hat{E}_{\mathrm{HF}} \rangle (t_1) = -\frac{\mathrm{i}}{2} \sum_{m,n=0}^{n_b-1} \Sigma_{mn}^{\mathrm{HF}}(t_1) g_{nm}^<(t_1, t_1), \tag{19}$$

and the correlation energy $\langle \hat{E}_{\mathrm{corr}} \rangle (t_1) = -\frac{\mathrm{i}}{2} \int_\mathcal{C} \mathrm{d}\bar{t} \, \mathrm{Tr} \{ \mathbf{\Sigma}^{\mathrm{corr}}(t_1, \bar{t}) \mathbf{g}(\bar{t}, t_1^+) \}$.

Other interesting quantities are, e.g., the time-dependent dipole moment $\langle \hat{d} \rangle (t_1) = -\mathrm{i} e \int \mathrm{d}^\mathrm{d} r_1 \{ \mathbf{r}_1 G^<(\mathbf{r}_1 t_1, \mathbf{r}_{\bar{1}} t_1) \}_{\mathbf{r}_1 = \mathbf{r}_{\bar{1}}}$ or the one-particle spectral function [3] $a(\omega, t_{\mathrm{c.m.}}) = \mathrm{i} \sum_m \int \mathrm{d}t_{\mathrm{rel.}} \mathrm{e}^{\mathrm{i}\omega t_{\mathrm{rel.}}} [g_{mm}^>(t_1, t_{\bar{1}}) - g_{mm}^<(t_1, t_{\bar{1}})]$.

## 5. Numerical results

In this section, we study the dynamical properties of a three-electron AA, when, initially in thermodynamic equilibrium, the system is excited by a single few-cycle laser pulse described in the dipole approximation, cf equation (3). More precisely, the field is linearly polarized in the $x$-direction and has the time dependence

$$\gamma(t) = \mathcal{E}_0 \, \mathrm{e}^{-(t-t_l)^2/(2\tau_l^2)} \cos(\omega_l (t - t_l)), \tag{20}$$

where $\mathcal{E}_0 = \mathcal{E}_l / \sqrt{2\pi}$ denotes the amplitude of the electric field, the Gaussian envelope is centered at $t_l$, the pulse duration (variance) is given by $\tau_l$, and the oscillation frequency is $\omega_l$; cf figures 3(*a*)–(*c*).

As the response characteristics $\Xi(\omega_l)$ of the quantum system we define the amount of energy that has been absorbed from the laser field for a fixed frequency $\omega_l$, i.e.

$$\Xi(\omega_l) = \langle \hat{E}_{\mathrm{tot}} \rangle_{\omega_l} (t \to \infty) - \langle \hat{E}_{\mathrm{tot}} \rangle (0). \tag{21}$$

This quantity together with the time-dependent occupation probabilities $\langle \hat{n}_m \rangle (t)$ allows for the determination of (off)resonant nonequilibrium behavior (and nonlinear effects); see sections 5.1 and 5.2.

The nonequilibrium behavior of the quantum system (1) is theoretically well known. Driven by the laser field, the AA exactly responds according to the excitation of the center-of-mass (Kohn or sloshing) mode. This is obtained from the Kohn theorem, and its generalization to the case of an additional external dipole field; see [22] and references therein. Its statement is that, independent of dimensionality, the center-of-mass coordinate $\mathbf{R}(t) = N^{-1} \sum_i \mathbf{r}_i(t)$ of a parabolically confined, interacting electron system performs (equivalently to a single particle in the AA) the motion of a forced harmonic oscillator, $|\ddot{\mathbf{R}}| + \omega_0^2 |\mathbf{R}| = N e E(t) / m_e^*$. Furthermore,

this effect is accompanied by a rigid translation of the density profile $\langle\hat{n}\rangle(\mathbf{r})$, since the particle interaction appears only in the relative Hamiltonian and $[H_{\text{c.m.}}, H_{\text{rel.}}] = 0$. The key point in the present study is, however, that the Kohn theorem also holds when the interaction is treated approximately, as long as density, total energy and momentum are preserved (the conserving approximation), and also applies to zero and finite temperatures—for the proof see [22].

The following mean-field results for 1D and 2D have been obtained from NEGF calculations with up to $n_b = 40$ HF orbitals. The main limitations of the approach are thereby (i) the basis size, which sets the dimension of the time-evolution matrix $\mathbf{U}(t_1) = \exp(-\mathrm{i}[\mathbf{h}(t_1) + \mathbf{\Sigma}^{\text{HF}}(t_1)]t_1)$ to be computed in each time step (diagonalizing $\mathbf{h} + \mathbf{\Sigma}^{\text{HF}}$), and (ii) the two-electron integrals $w_{ij,kl}$, equation (15), that generally require large memory resources (scaling with $n_b^4$) and need to be processed very frequently in the self-energy expression $\mathbf{\Sigma}(t_1, t_{\bar{1}})$. With more than 50 000 time steps needed to achieve convergence, this results in computing times of typically several hours on a single machine. For the correlated time evolution of the AA in the second Born approximation, the propagation must be carried out in the whole two-time plane $(t_1, t_{\bar{1}})$. This is an even more intricate task as one needs to compute all the higher-order collision integrals on the rhs of the KBE. However, these calculations are currently near completion—examples are to be found in [17], and for applications on real atoms and small molecules see [18, 20, 21].

### *5.1. The 1D case*

For the 1D AA calculations in equilibrium and nonequilibrium, we, in equation (15), have replaced the pure Coulomb interaction $w(x - \bar{x})$ by $\lambda[(x - \bar{x})^2 + \alpha^2]^{-1/2}$ with $\alpha = 0.1$ as a regularization parameter. This is necessary to make the integrals $w_{mn,kl}$ finite[1] and, in a physical interpretation, allows for a small transversal spread of the wavefunction [2]. For $\alpha \lesssim 0.1$, all considered quantities are found to be converged, whereas for $\alpha \approx 1$, screening effects are expected to be large leading to lower total energies. In 2D, we used $\alpha \equiv 0$ as the integrals converge.

We consider three electrons in a 1D artificial atom at $\beta = 2$. With $\lambda = 2.0$ the system is tuned into the crossover regime between Fermi liquid-like and crystal-like behavior. The equilibrium properties can be read from figure 2 for the HF and second Born approximation. For the HF energy spectrum and the corresponding distribution function $f_\beta(\epsilon_m - \mu)$ of the equilibrium (initial) state, including its collisional renormalization in the second Born approximation, see figure 2(*a*). The one-electron density $\langle\hat{n}\rangle(x)$ is displayed in figure 2(*b*). Compared to the HF result (the solid curve, $\langle\hat{E}_{\text{tot}}^{\text{HF}}\rangle = 8.790$), here the inclusion of electron–electron scattering (the dashed curve, $\langle\hat{E}_{\text{tot}}^{\text{2ndB}}\rangle = 8.941$) leads to a considerable reduction of the density modulation, which is accompanied by an increase of the total energy of about 1.7%.

Starting from the HF Green's function $G^M(\mathbf{r}_1, \mathbf{r}_{\bar{1}}; \tau)$, the AA was now propagated in time under the presence of a laser field (centered at $t_l = 25$) with amplitude $\mathcal{E}_l = 0.5$ and frequency $\omega_l = 1.25\omega_0$. What happens to the orbital occupations and the energies for different pulse durations $\tau_l$ is shown in figures 3 and 4. In all cases, gradually, the HF orbitals $m < 3$ become depopulated and the states $m \geqslant 3$ analogously become populated with the preservation of $N(t)$. Oscillations of the increased total, kinetic and potential energy, and $\langle\hat{n}_m\rangle(t)$ thereby occur with twice the confinement frequency. In figures 3(*a*) and 4(*a*), respectively, the laser excitation is such that the $N$-particle dynamics is decelerated after the pulse has passed. Consequently, we

[1] In homogeneous systems, the integrals appearing in the interaction kernel (the rhs of equations (12) and (13)) may diverge at large electron–electron distances $\mathbf{r}_1 - \mathbf{r}_{\bar{1}}$. However, in finite systems, this is generally not the case since the one-electron density $\langle\hat{n}\rangle(\mathbf{r}_1)$ vanishes for $\mathbf{r}_1 \to \infty$.

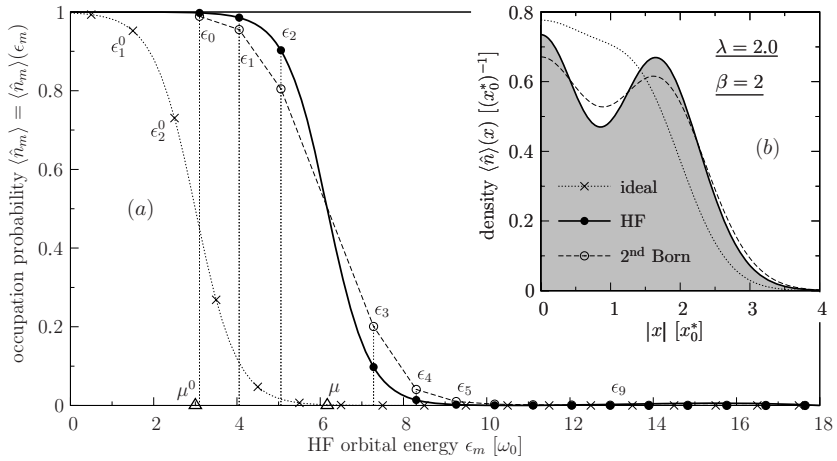


**Figure 2.** Thermodynamic properties of $N = 3$ charge carriers in the 1D AA with $\lambda = 2.0$ and $\beta = 2$. $(a)$ HF distribution function $f_\beta(\epsilon_m - \mu)$ (the solid curve) and renormalization at the second Born level (the dashed curve). For comparison, the dotted curve shows the ideal system ($\lambda \equiv 0$) with energies $\epsilon_m^0 = m + 1/2$. The triangle marks the position of the HF (ideal) chemical potential $\mu = 6.1692$ ($\mu^0 = 2.9989$). $(b)$ Density profile $\langle \hat{n} \rangle(x)$ for the ideal system as well as for the HF and second Born approximation.

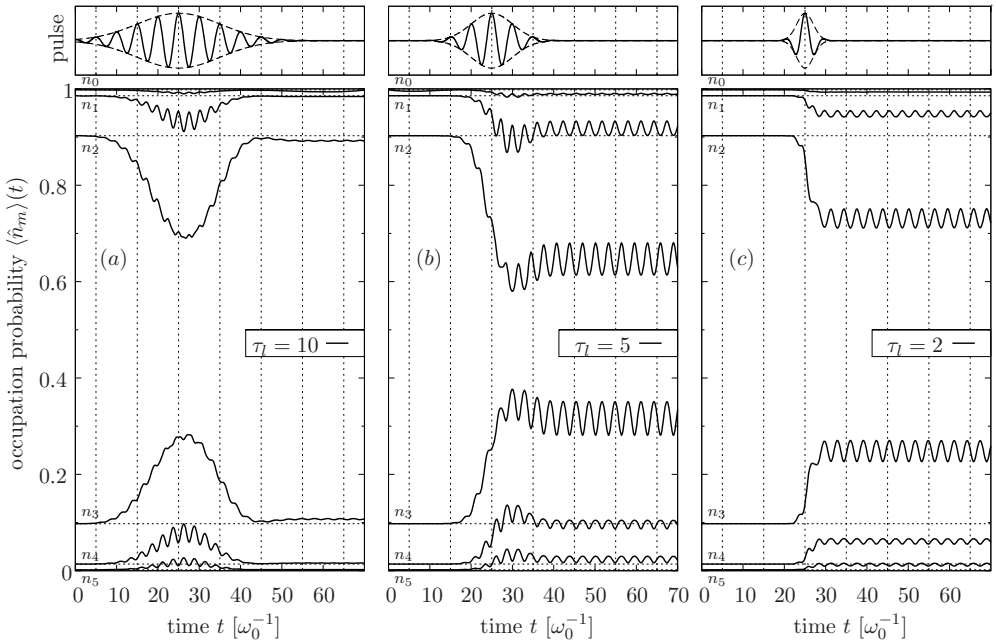


**Figure 3.** Nonequilibrium behavior of the $N = 3$ AA system (1D) with parameters $\lambda = 2.0$ and $\beta = 2$. $(a)$–$(c)$ show the mean-field dynamics of the HF orbital occupation probabilities $\langle n_i \rangle(t)$ at a near-resonant laser frequency $\omega_l = 1.25\omega_0$ and three different pulse durations $\tau_l$. The corresponding pulse shapes $\gamma(t)$ are indicated above the figures.

nearly recover the initial state characterized by $\langle \hat{n}_m \rangle(0)$ and $\langle \hat{E}_{\text{tot}} \rangle(0)$. Also, for different pulse durations, i.e. different spectral profiles of the laser, the maximum laser energy absorption

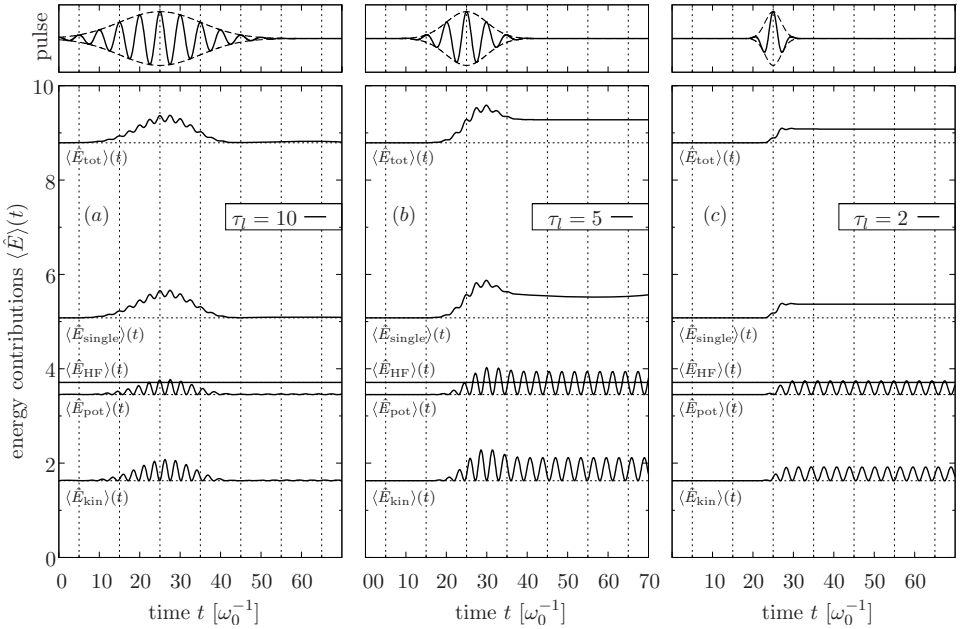


**Figure 4.** For the laser-irradiated artificial atom [$\omega_l = 1.25\omega_0$] also considered in figure 3, (*a*)–(*c*) show the mean-field dynamics of the relevant energy contributions in dependence of the pulse duration. For $\tau_l = 10$, the AA returns after the excitation is almost into its initial state (off-resonant situation). Whereas, in figures (*b*) and (*c*) the spectral width of the laser frequency is essentially increased compared to (*a*), leading to the AA remaining in an excited state of the Kohn mode (the resonant case). Potential and kinetic energies thereby oscillate out of the phase with exactly double confinement frequency $\omega_0$, while the HF energy stays constant.

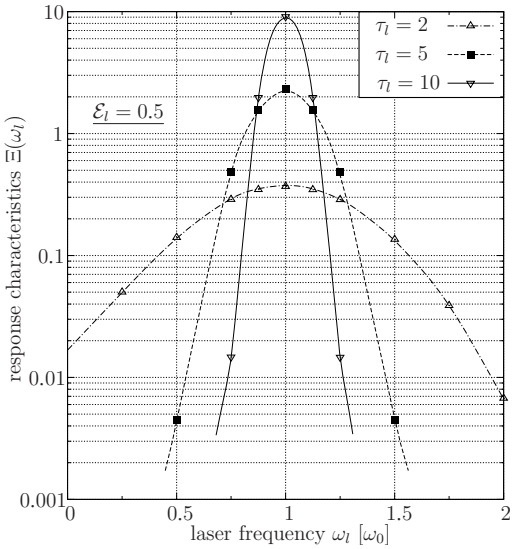


**Figure 5.** Response characteristics $\Xi(\omega_l)$, equation (21), for the pulsed-laser excitation of $N = 3$ electrons in the 1D artificial atom. The system parameters are as in figure 2. The AA shows resonance behavior at the confinement frequency only, i.e. for $\omega_l = \omega_0$, and responds via the c.m. motion (Kohn mode)—rigid translation of the whole density. With increasing pulse durations $\tau_l$ (sharpened laser frequency) the resonance curves become more and more peaked.

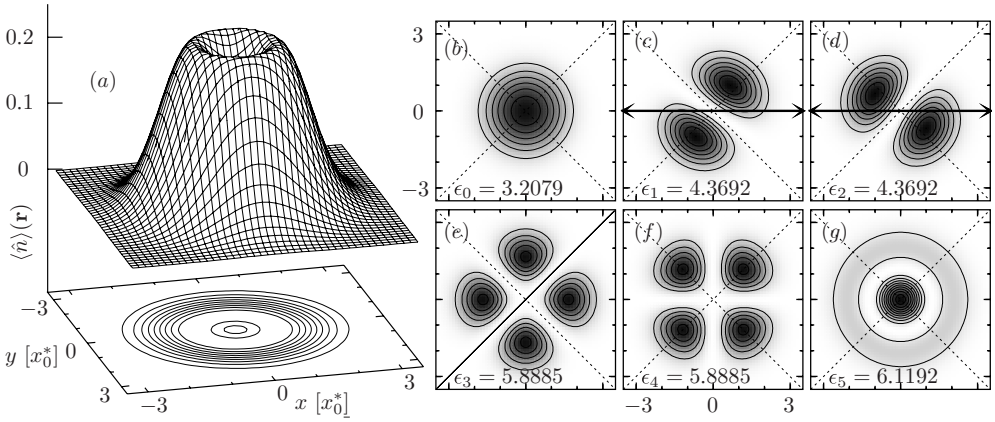


**Figure 6.** Thermodynamic initial state of the 2D artificial atom ($N = 3$) at $\lambda = 2.0$ and $\beta = 2$ (in the HF approximation). (*a*) Single-electron density profile $\langle\hat{n}\rangle(\mathbf{r})$ which is rotationally symmetric. (*b*)–(*g*) Energetically lowest spatial, HF states $\phi_m(\mathbf{r})$ with orbital energies $\epsilon_0, \ldots, \epsilon_5$ where $\epsilon_1$ and $\epsilon_2$ as well as $\epsilon_3$ and $\epsilon_4$ are degenerate. The arrows in (*c*) and (*d*) mark the direction of polarization of the laser field $\gamma(t)$, equation (20).

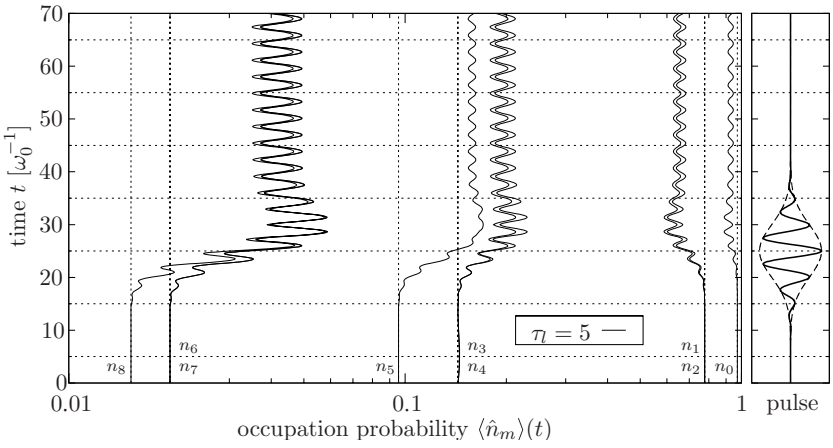


**Figure 7.** Mean-field dynamics of the HF orbital occupation probabilities $\langle\hat{n}_m\rangle(t) = n_m$ for three charge carriers in a 2D artificial atom with the coupling parameter $\lambda = 2.0$ and inverse temperature $\beta = 2$. The laser frequency is again near resonant, $\omega_l = 1.25\omega_0$, and the pulse duration is $\tau_l = 5$. In the initial state the occupation numbers $n_1$ and $n_2$, $n_3$ and $n_4$ as well as $n_6$ and $n_7$ are practically pairwise degenerate, compare with the energy spectrum displayed in figure 6.

is observed at the confinement frequency $\omega_0$, cf the response function $\Xi(\omega_l)$ in figure 5. In addition, the single resonance peak at $\omega_l = \omega_0$ sharpens with the increase of $\tau_l$. Consider now the spatial dynamics. We observe in all cases that the center of mass of the AA, $\mathbf{R}(t)$, performs a harmonic oscillation with frequency $\omega_0$ while the whole density profile itself is translated rigidly. Accompanying this fact, $E_{\mathrm{HF}}$ is constant in time; see figure 4. Thus, we numerically confirm that the Kohn theorem is satisfied.

### *5.2. The 2D case*

For the three-electron AA in 2D, we have chosen the same system parameters, $\lambda = 2.0$ and $\beta = 2$—however, no regularization parameter $\alpha$ was needed in the two-electron integrals $w_{mn,kl}$. The (almost) rotationally symmetric density profile for the equilibrium state is shown in figure 6 and indicates a ring-like structure. It is instructive to note that the HF solution of the Dyson equation leads to orbitals $\phi_m(\mathbf{r})$ that are in general arbitrarily oriented in space; compare figures 6(*b*)–(*g*). Together with the energetically degenerate states $m = 1$ and 2 ($m = 3$ and 4, etc), this has the following consequence on the dipole excitation. As degenerate orbitals can be differently oriented relative to the laser field, in the time evolution of the artificial atom this degeneracy is lifted. In the present case, the orbitals $m = 1$ and $m = 2$ (see figures 6(*c*) and (*d*)) are almost aligned with the diagonals (dotted lines), nevertheless the small deviations are sufficient to clearly influence the evolution of the occupation numbers $\langle \hat{n}_m \rangle(t)$; see $\langle \hat{n}_1 \rangle$ and $\langle \hat{n}_2 \rangle$ as well as $\langle \hat{n}_3 \rangle$ and $\langle \hat{n}_4 \rangle$ in figure 7.

## 6. Conclusion and outlook

We have presented an analysis of femtosecond relaxation of few-particle artificial atoms during and after a short laser pulse. The method of NEGF was shown to be efficient to describe the dynamics even in the range of strong Coulomb correlations. The numerical solution of the KBE reveals that the c.m. (Kohn or sloshing) mode is well reproduced already for the most simple many-body ansatz, the HF approximation. Besides partial compensation of interband transitions, we expect no qualitative change in the presented results, when higher order effects, e.g. correlations at the second Born level, are being included during time propagation. The amount of compensation is thereby determined by the influence of correlations on the one-electron spectrum [3] which undergoes shifting and broadening in the discrete HF energies. Moreover, the collisional renormalization is typically small for quantum systems in traps [3, 17].

Numerically, the c.m. mode excitation can serve as a very sensitive test for the NEGF calculation (and any other numerical code) involving quantum many-body approximations [22]. To investigate the correlated dynamics within the frame of the second Born approximation is the subject of ongoing work.

## Acknowledgments

We acknowledge stimulating discussions with R van Leeuwen, A Filinov and S Bauch. This work was supported by the Innovationsfond Schleswig-Holstein.

## References

[1] Ashoori R C 1996 *Nature* **379** 413
[2] Jauregui K, Häusler W and Kramer B 1993 *Europhys. Lett.* **24** 581–7
[3] Balzer K, Bonitz M, van Leeuwen R, Dahlen N E and Stan A 2008 *Phys. Rev.* B submitted (arXiv:cond-mat/08102425)
[4] Wineland D J, Bergquist J C, Itano W M, Bollinger J J and Manney C H 1987 *Phys. Rev. Lett.* **59** 2935
[5] Brey L, Johnson N F and Halperin B I 1989 *Phys. Rev.* B **40** 10647
[6] Filinov A V, Bonitz M and Lozovik Yu E 2001 *Phys. Rev. Lett.* **86** 3851
Filinov A V, Lozovik Yu E and Bonitz M 2000 *Phys. Stat. Sol.* (b) **221** 231
[7] Kouwenhoven L P, Austing D G and Tarucha S 2001 *Rep. Prog. Phys.* **64** 701
[8] Jefferson J H and Häusler W 1997 arXiv:cond-mat/9705012
[9] de Heer W A 1993 *Rev. Mod. Phys.* **65** 611

[10] Manninen M and Reimann S M 2007 arXiv:cond-mat/0703292
[11] Bonitz M 1998 *Quantum Kinetic Theory* (Stuttgart: B G Teubner)
Kremp D, Bornath Th, Bonitz M and Schlanges M 1999 *Phys. Rev.* E **60** 4725
[12] Keldysh L V 1964 *Zh. Eksp. Teor. Fiz.* **47** 1515
Keldysh L V 1965 *Sov. Phys.—JETP* **20** 235
[13] Kadanoff L P and Baym G 1962 *Quantum Statistical Mechanics* (New York: Benjamin)
[14] Kraeft W D, Kremp D, Ebeling W and Röpke G 1986 *Quantum Statistics of Charged Particle Systems* (Berlin: Akademie Verlag)
[15] van Leeuwen R, Dahlen N E and Stan A 2006 *Phys. Rev.* B **74** 195105
Kwong N H and Bonitz M 2000 *Phys. Rev. Lett.* **84** 1768
[16] Stan A, Dahlen N E and van Leeuwen R 2006 *Europhys. Lett.* **76** 298
[17] Balzer K 2007 *Diploma thesis*, Kiel University http://www.theo-physik.uni-kiel.de/~bonitz
[18] Dahlen N E and van Leeuwen R 2005 *J. Chem. Phys.* **122** 164102
[19] Ludwig P, Balzer K, Filinov A, Stolz H and Bonitz M 2008 *New. J. Phys.* **10** 083031
[20] Dahlen N E, van Leeuwen R and Stan A 2006 *J. Phys: Conf. Ser.* **35** 340–8
[21] Dahlen N E and van Leeuwen R 2007 *Phys. Rev. Lett.* **98** 153004
[22] Bonitz M, Balzer K and van Leeuwen R 2007 *Phys. Rev.* B **76** 045341